Production and Characterisation of D3cpv, a FRET-Based Calcium Sensor, and Application in HeLa Cells

Amedeo Leproni, November 2023

Biotechnology MPhil Practical Lab Course

Key techniques: Gibson assembly, Ni affinity chromatography (FPLC), microplate FRET assay, HeLa transfection, FLIM

Abstract.

D3cpv is a genetically encoded calcium indicator composed of CFP and YFP linked by a calcium-binding motif. Calcium binding drives a conformational change that increases Förster resonance energy transfer (FRET) from CFP to YFP, enabling optical readout of Ca^{2+} state. This report describes an end-to-end pipeline to (i) assemble a bacterial expression plasmid encoding D3cpv, (ii) express and purify His-tagged D3cpv from Escherichia coli using nickel affinity chromatography on an FPLC system, (iii) quantify calcium-dependent behaviour in vitro using a $CaCl_2$ titration in a microplate assay, and (iv) express D3cpv in HeLa cells for fluorescence lifetime imaging microscopy (FLIM)-based FRET analysis. Molecular cloning was validated by agarose gel electrophoresis, colony screening, and Sanger sequencing with high pairwise identity to the designed D3cpv sequence. Induced bacterial cultures showed increased expression of D3cpv at the expected molecular weight, while the purified sample contained a dominant lower-molecular-weight species, suggesting loss of mass during purification or co-purification of an alternative protein. Microplate titration measurements produced a calcium response curve that could be fitted to a Hill function, though extracted parameters deviated from literature values. In cells, FLIM-derived FRET efficiencies distinguished wild-type from mutant D3cpv in aggregate, but variability across imaged cells and pharmacological perturbations limited interpretability. Overall, the pipeline demonstrates successful upstream construct generation and expression, while downstream quantitative characterisation benefits from optimisation of purification integrity, expression levels, and cellular transfection performance.

Table of contents

1. Introduction

Intracellular Ca^{2+} is a ubiquitous second messenger involved in diverse signalling pathways. Genetically encoded calcium indicators offer a non-destructive way to quantify calcium dynamics in living systems. D3cpv is a FRET-based sensor in which a CFP donor and YFP acceptor flank a calcium-binding motif. Upon Ca^{2+} binding, CFP and YFP are brought within Förster distance, increasing FRET efficiency. Excitation of CFP (436 nm) yields CFP emission (488 nm) and, via FRET, YFP emission (528 nm). The ratio of acceptor to donor signal (528 nm to 488 nm) provides a readout related to calcium state.

A stage-gated workflow was adopted to prevent downstream work from proceeding on unvalidated intermediates. The pipeline comprised: (i) molecular cloning of a pET24b-based expression plasmid encoding D3cpv, (ii) bacterial expression and purification of His-tagged D3cpv, (iii) in vitro $CaCl_2$ titration to infer binding behaviour, (iv) HeLa transfection with wild-type and mutant constructs, and (v) FLIM-based estimation of FRET efficiency in cells.

2. Materials and Methods

Work was performed across a two-week taught practical series. Each stage is described with a short rationale followed by execution details, reflecting the chronological progression of the project.

2.1 Key buffers and reagents

Buffer	Composition	Purpose
Lysis buffer	50 mM HEPES, 300 mM NaCl, 10% glycerol, protease inhibitors	Solubilisation and stabilisation of His-tagged D3cpv during cell lysis
Ni column wash / equilibration	50 mM HEPES, 300 mM NaCl, 10% glycerol, low imidazole	Promote specific binding of His-tagged protein and remove weak binders
Ni column elution	50 mM HEPES, 300 mM NaCl, 10% glycerol, 200 mM imidazole	Competitive elution of His-tagged D3cpv from Ni resin
Assay buffer	10 mM MOPS, 100 mM KCl, pH 7.2	In vitro Ca2+ titration and fluorescence measurements

Table 1. Buffer compositions used for expression, purification, and in vitro characterisation.

2.2 Molecular cloning of pET24b-D3cpv

D3cpv was assembled into a bacterial expression plasmid to enable high-yield recombinant production. PCR amplification and fragment verification preceded assembly to ensure correct fragment sizes and sufficient DNA yield.

CFP, YFP, and pET24b backbone fragments were amplified by high-fidelity PCR using primers designed with overlapping ends for Gibson assembly. Products were verified by agarose gel electrophoresis, excised, and purified. Purified fragments were quantified by nanodrop and assembled by Gibson assembly into a circular plasmid. Assembled plasmid was transformed into E. coli, plated on LB agar containing kanamycin, and colonies were screened by colony PCR. A positive colony was expanded, plasmid DNA was prepared, quantified, and validated by Sanger sequencing with in silico alignment to the designed D3cpv sequence.

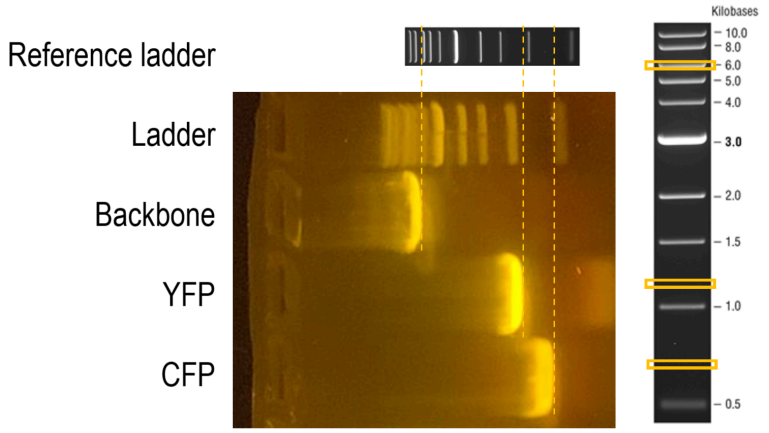

Figure 1. Agarose gel electrophoresis of PCR-amplified CFP, YFP, and pET24b backbone fragments. Band positions were compared to a DNA ladder to verify expected product sizes prior to assembly.

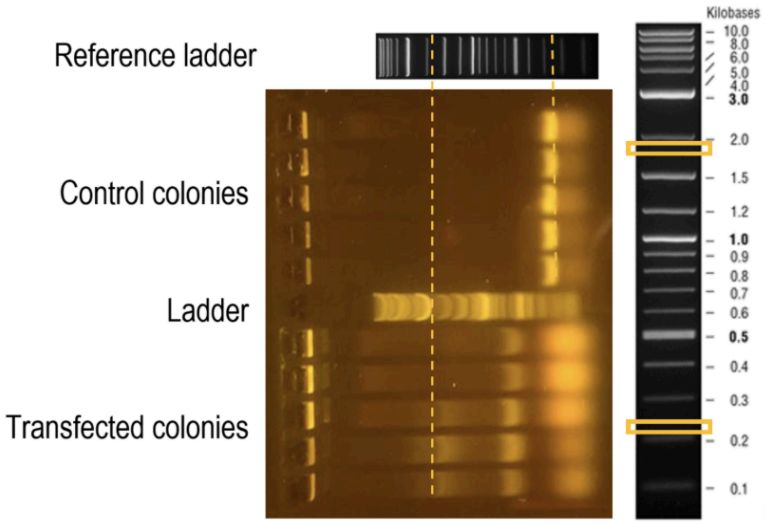

Figure 2. Colony PCR screening of candidate transformants and negative control colonies following Gibson assembly and bacterial transformation. Bands at the expected size for the D3cpv insert (~2 kb) were observed in selected colonies, which were subsequently expanded for plasmid preparation and sequencing.

2.3 Bacterial expression and nickel affinity purification of D3cpv

Recombinant D3cpv was expressed in an IPTG-inducible E. coli strain and purified via its His-tag using nickel affinity chromatography on an FPLC system. SDS-PAGE was used to assess expression and purification quality prior to functional assays.

Verified pET24b-D3cpv plasmid was transformed into an expression strain. Cultures were grown in LB containing kanamycin at 37 °C with shaking until mid-log phase (OD_{600} within

0.4 to 0.8). Expression was induced with IPTG to 1 mM final concentration and continued for 3 to 4 hours at 30 °C. Non-induced and induced samples were collected for SDS-PAGE. Cells were harvested by centrifugation (3500 g, 15 min, 4 °C) and pellets were processed for lysis in a HEPES-based lysis buffer. Lysates were clarified by centrifugation and loaded onto a Ni2+ affinity column on an FPLC system. After washing, bound protein was eluted with an imidazole-containing buffer. Eluted fractions were assessed by SDS-PAGE and pooled for downstream use.

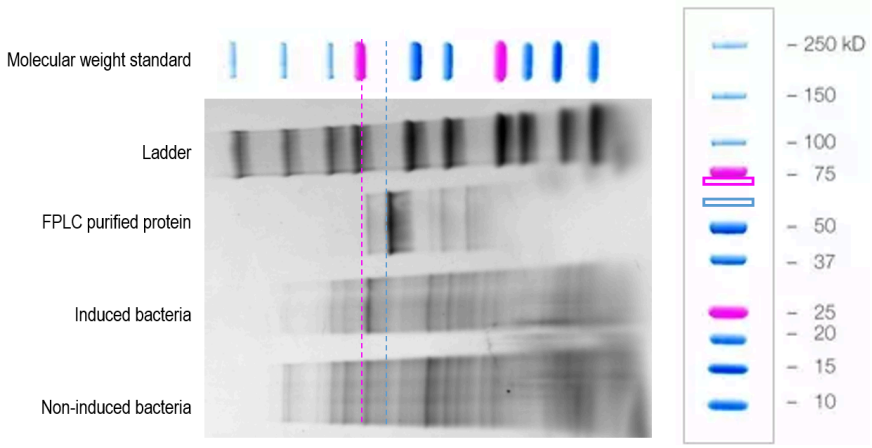

Figure 3. SDS-PAGE analysis of bacterial lysates (non-induced and IPTG-induced) and FPLC-purified protein following nickel affinity chromatography. IPTG induction increases abundance of a band near the expected molecular weight of D3cpv (~74 kDa), while the purified fraction is dominated by a lower-molecular-weight species, indicating preferential enrichment of a truncated or alternative protein product.

2.4 Buffer exchange and preparation for in vitro assay

Imidazole and purification salts can perturb fluorescence measurements and calcium binding. Purified protein was exchanged into MOPS-based assay buffer prior to titration. Pooled protein was desalted into an assay buffer (10 mM MOPS, 100 mM KCl, pH 7.2) using a desalting column. Buffers were prepared to minimise adventitious divalent ions, and solutions used for the $CaCl_2$ series were prepared in the same buffer to maintain constant ionic strength.

2.5 In vitro $CaCl_2$ titration and microplate FRET assay

Calcium-dependent conformational change in D3cpv alters FRET from CFP to YFP. A $CaCl_2$ titration series enables extraction of apparent binding behaviour by fitting the ratio response to a Hill function.

A $CaCl_2$ stock solution (2000 uM) was used to prepare a titration series spanning sub-micromolar to millimolar concentrations in an assay buffer. In each well, 50 uL of $CaCl_2$ stock solution at the indicated concentration was mixed with 50 uL of either purified D3cpv solution or assay buffer. This produced final $CaCl_2$ concentrations at half the labelled stock values. Protein-containing wells and matched buffer-only wells were arranged in parallel for background subtraction. Fluorescence was measured using excitation at 436 nm and emission readings at 480 nm (CFP) and 520 nm (YFP). The acceptor-to-donor ratio was calculated after background correction and fitted to a Hill function.

$CaCl_2$ stock (uM)	Final $CaCl_2$ in well (uM)
2000	1000
1500	750
1000	500
200	100
150	75
100	50
20	10
15	7.5
10	5
2	1
1.5	0.75
1	0.5
0.2	0.1
0.1	0.05
0.02	0.01
0	0

Table 2. $CaCl_2$ titration series used for the microplate assay. Final concentrations reflect 1:1 mixing of $CaCl_2$ stock with protein or buffer.

Figure 4. Microplate layout for in vitro $CaCl_2$ titration assay. Numbers indicate $CaCl_2$ stock concentrations (uM). Each well contained 50 uL of $CaCl_2$ stock solution mixed with 50 uL of either purified protein solution or MOPS buffer, yielding final $CaCl_2$ concentrations equal to half the displayed values. Protein-containing wells and buffer-only controls were arranged in parallel to enable background subtraction and assay validation.

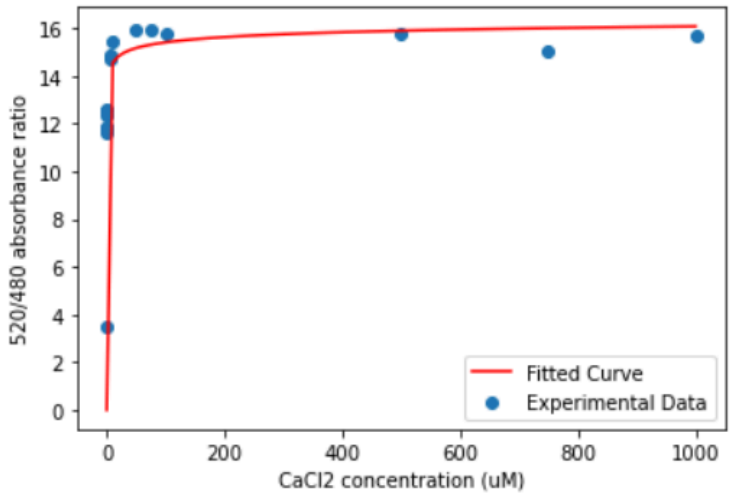

Figure 5. Acceptor-to-donor fluorescence ratio (520/480) of purified D3cpv across a $CaCl_2$ titration series, fitted to a Hill function to extract apparent binding parameters.

2.6 HeLa cell culture, transfection, and pharmacological perturbations

Cellular measurements test sensor behaviour in a physiological environment and provide a route to infer intracellular Ca2+ changes. Wild-type and mutant D3cpv constructs provide a functional and non-functional comparison for FLIM-based FRET analysis.

HeLa cells were maintained under standard incubator conditions (37 C, 5% CO2) and prepared for transfection by washing, resuspension, and counting. Cells were seeded into an 8-well chamber and cultured overnight. D3cpv plasmid DNA was complexed with a lipid-based transfection reagent and added to six wells; mutant construct was added to two wells. After 24 hours of expression, two wells were treated with ionomycin to increase intracellular calcium and two wells were treated with BAPTA to reduce intracellular calcium, prior to imaging.

2.7 FLIM acquisition and FRET efficiency calculation

FLIM quantifies donor lifetime, which decreases in the presence of FRET. FRET efficiency E was calculated using E = 1 - (tau_FRET / tau_nonFRET), where tau is the mean donor lifetime.

Chamber slides were mounted on a microscope equipped for time-correlated single photon counting. Cells were imaged under controlled environmental conditions, and lifetime decays

were fitted to extract mean tau values. Wild-type and mutant samples were analysed in parallel, and fit quality was assessed using chi2.

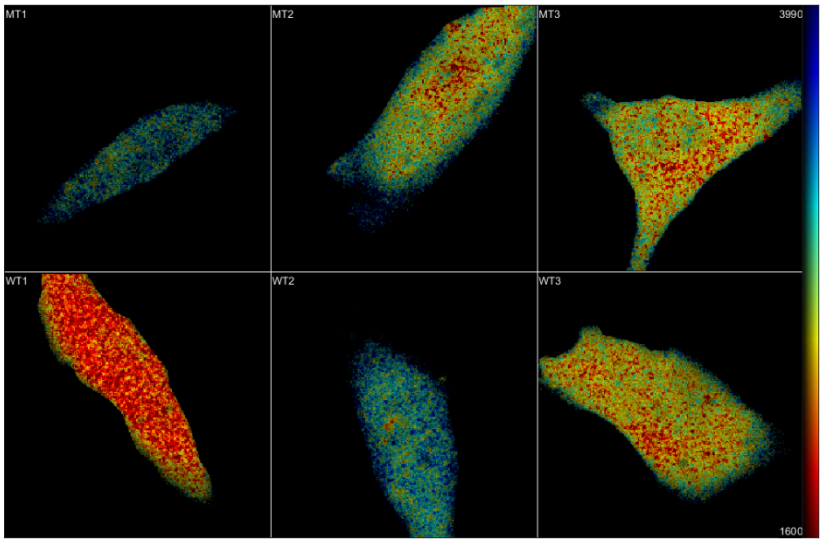

Figure 6. Representative fluorescence lifetime imaging microscopy (FLIM) maps for HeLa cells expressing wild-type (WT) and mutant (MT) D3cpv. Pixel-wise donor lifetimes were fitted to extract mean fluorescence lifetimes, which were used to calculate FRET efficiencies.

3. Results

3.1 PCR verification and DNA yields

PCR amplification produced bands consistent with the expected fragment sizes for CFP (approximately 700 bp), YFP (approximately 1200 bp), and the pET24b backbone (approximately 6000 bp) (Figure 1). Nanodrop quantification indicated adequate yield for CFP and YFP, while the backbone yield was low and was replaced with a prepared backbone prior to assembly (Table 3).

DNA fragment	Nanodrop concentration (ng/uL)
CFP	32.7
YFP	43.0
Backbone (pET24b)	5.9

Table 3. Nanodrop concentrations of gel-purified PCR fragments used for assembly.

3.2 Colony screening and sequence validation

Colony PCR identified two candidate transformants with an insert band at the expected size for D3cpv (approximately 2000 bp), while controls showed only short amplicons (Figure 2). Insert DNA from Alpha1 and Alpha2 was quantified (Table 4), and Alpha2 was selected for sequencing due to higher yield. Sanger sequencing produced two reads of approximately 1000 bases each, with pairwise identity of 99.64% and 98.53% relative to the designed sequence, confirming successful assembly of pET24b-D3cpv.

Colony	Insert concentration (ng/uL)	260/280 ratio
Alpha1	66.5	1.87
Alpha2	79.2	1.89

Table 4. Quantification and purity ratios of insert DNA from candidate colonies.

3.3 Expression and purification assessment

SDS-PAGE of non-induced and IPTG-induced lysates showed a band at the expected D3cpv molecular weight (74.4 kDa), with increased intensity after induction, consistent with inducible expression (Figure 3). The purified fraction contained a dominant band at approximately 64 kDa, with a fainter band at the expected D3cpv molecular weight, indicating that the purified material was enriched for a lower-molecular-weight species.

3.4 In vitro CaCl2 titration and fitted parameters

The microplate assay yielded a calcium-dependent change in the acceptor-to-donor ratio that could be fitted using a Hill function (Figure 5). Extracted parameters are summarised in Table 5.

Parameter	Value
Hill coefficient (nH)	0.150
Dissociation constant (Kd, uM)	0.000464
Binding affinity (1/Kd)	2155.17

Table 5. Apparent binding parameters from Hill fitting of the calcium titration curve.

3.5 Cellular FLIM-based FRET

FLIM analysis produced mean donor lifetimes and derived FRET efficiencies for mutant and wild-type D3cpv (Table 6). Across the sampled cells, wild-type D3cpv displayed higher FRET efficiency than mutant, consistent with functional energy transfer in the wild-type sensor (Figure 6).

Condition	Cell 1 tau (ns)	Cell 2 tau (ns)	Cell 3 tau (ns)	Mean tau (ns)	FRET efficiency (%)
Mutant	2.81	2.58	2.42	2.60	0.781
Wild type	2.00	2.92	2.37	2.40	8.42
Non-FRET reference				2.62	
Mean fit chi2				1.24	

Table 6. Donor lifetimes (tau) and derived FRET efficiencies from FLIM fitting.

Pharmacological perturbations using ionomycin and BAPTA were explored qualitatively; responses were variable and did not produce a consistent shift in FLIM-derived FRET relative to untreated wild-type cells.

4. Discussion

This work implemented a complete production pipeline for a genetically encoded calcium biosensor, with validation checkpoints at each stage. Upstream cloning was robust: PCR products matched expected sizes, colony screening identified correct transformants, and sequencing confirmed high identity with the designed D3cpv sequence. These results support successful assembly of pET24b-D3cpv and provide a reliable starting point for downstream expression work.

Expression analysis showed inducible enrichment of a band at the expected molecular weight (74.4 kDa), consistent with IPTG-driven D3cpv expression. However, the purified fraction was dominated by a lower-molecular-weight species (approximately 64 kDa), suggesting either partial proteolysis or co-purification of a non-target protein. Loss of approximately 10 kDa is compatible with cleavage of one fluorescent domain or truncation of the sensor, which would be expected to perturb FRET behaviour and reduce the functional fraction of protein in vitro.

In vitro titration produced a fitted Kd of 0.000464 uM and a Hill coefficient of 0.15. These values deviate from literature reports for cameleon-type sensors, which typically exhibit micromolar-range apparent affinities and higher Hill coefficients. A plausible interpretation is that the assay readout was dominated by a subset of protein that saturates rapidly, potentially reflecting altered sensor integrity or an effective reduction in dynamic range. Improving purification integrity, confirming the identity of the purified species, and repeating titration using a preparation enriched for full-length D3cpv are expected to improve parameter estimates.

In cells, FLIM-based analysis yielded higher mean FRET efficiency for wild-type than mutant D3cpv, as expected for a functional sensor. Nonetheless, efficiencies were substantially below typical values reported in the literature for well-expressed cameleon sensors in mammalian cells. Qualitative inspection of lifetime maps indicated variability across cells and overlap between conditions, consistent with heterogeneous expression and variable cell state. The pharmacological perturbations did not shift FRET in the expected direction, suggesting that expression level, transfection efficiency, and experimental timing are key determinants of interpretability.

5. Conclusions

pET24b-D3cpv was assembled successfully and validated by gel electrophoresis, colony screening, and sequencing with high pairwise identity to the designed sequence.

IPTG induction increased expression of a protein band at the expected D3cpv molecular weight.

Nickel affinity purification enriched a dominant lower-molecular-weight species, motivating refinement of purification conditions and verification of purified protein identity.

A microplate $CaCl_2$ titration produced a measurable response curve and fitted parameters, though these deviated from literature values and are consistent with altered sensor integrity.

FLIM-based cellular measurements distinguished wild-type from mutant in aggregate, but variability and pharmacological perturbation responses indicate that optimisation of transfection and expression is required for quantitative intracellular calcium estimation.

6. Biotechnological interest of intracellular calcium sensing

Intracellular calcium is a central regulator of cellular signalling, linking external stimuli to processes such as secretion, contraction, gene expression, and excitability. Genetically encoded calcium sensors are therefore widely used in basic research, particularly in neuroscience, where they enable direct measurement of neuronal activity and circuit dynamics, as well as in cell biology to study signalling coordination and stress responses.

Calcium sensing also has strong translational relevance. Aberrant calcium signalling contributes to diseases including cancer, cardiac disorders, neurodegeneration, and immune dysfunction. In these settings, calcium reporters provide functional phenotypes that complement molecular measurements and are increasingly used in drug discovery, where they support high-content screening of pathway activity, efficacy, and toxicity in living cells.

In applied contexts, intracellular calcium dynamics are closely linked to cell health and productivity in mammalian expression systems. Genetically encoded calcium sensors therefore offer a route to monitor and optimise culture conditions in biomanufacturing, supporting improved robustness and yield in industrial cell-based processes.

7. References

Madeira C, et al. Fluorescence lifetime imaging microscopy and fluorescence resonance energy transfer from cyan to yellow fluorescent protein validates a method to cluster proteins on solid surfaces. Journal of Biomedical Optics. 2009;14(4).

Greotti E, et al. mCerulean3-based cameleon sensor to explore mitochondrial Ca2+ dynamics in vivo. iScience. 2019;16:340-355.

Gibson DG, et al. Enzymatic assembly of DNA molecules up to several hundred kilobases. Nature Methods. 2009;6:343-345.